RSC Applied Interfaces

PAPER

View Article Online
View Journal | View Issue

Cite this: *RSC Appl. Interfaces*, 2025, **2**, 1237

Encapsulating freezing point depressants in elastomeric coatings: effective and durable anti-icing and de-icing coatings

Harish Sivakumaran, Ratul Dasgupta* and Guruswamy Kumaraswamy

Preventing ice formation on surfaces (anti-icing) and easy removal of ice formed on surfaces (de-icing) are of great technological importance for aircraft and overhead power lines. This has typically been effected by the use of coatings. A wide variety of coatings have been reported that delay frost formation or that afford the removal of deposited ice. However, there is a need for coatings that simultaneously exhibit anti-icing and de-icing properties and that are robust to multiple freeze–thaw cycles. Here, we report a two-phase coating comprising a soft gel-phase swollen with freezing point depressant, encapsulated in a hydrophobic, rigid elastomeric matrix phase. Since the coating is comprised predominantly of the soft gel phase (70% by vol.) embedded in the rigid matrix (minority phase, 30% by vol.), it exhibits a low elastic modulus while maintaining good mechanical durability. This coating exhibits exceptional performance, with an unprecedented combination of frost inhibition and removal of surface ice at very low stresses when compared with previously reported coatings. In particular, frosting takes over 200 minutes for a surface temperature of −20 °C at ambient conditions of 28 °C and 60% RH, compared to less than 20 minutes for superhydrophobic or liquid-infused slippery coatings. Further, these coatings are characterized by an adhesion stress ≈10 kPa, lower than even that for stress localized surfaces (≈40–50 kPa). Additionally, the anti-icing and de-icing performance of this coating is robust to multiple freeze–thaw cycles. In contrast to previously reported elastomeric coatings, de-icing is not due to stress localization – rather, it likely arises from local melting of deposited ice at the interface with the coating, by the action of the freezing point depressant. We attribute the exceptional performance of the coating to a combination of the overall low elastic modulus of the coating, with the slow release of hydrophilic freezing point depressant through the matrix.

Received 23rd June 2025,
Accepted 30th July 2025

DOI: 10.1039/d5lf00181a

rsc.li/RSCApplInter

Introduction

In several applications, it is necessary to prevent the formation of ice on surfaces, and to ensure low ice adhesion strength so that ice deposited on surfaces can be readily removed.[1–4] For example, ice formation on overhead power cables or on aircraft is undesirable and can result in adverse outcomes. Power outages have resulted from deposition of ice on power lines in cold climates.[5] An aircraft crash into the ocean, with the unfortunate loss of everyone on board, was attributed to obstructed pitot tubes due to ice formation during flight (page 17 of investigation report[6]), that gave conflicting flight speed data.[7,8] Given the broad technological importance of this problem, the formation of ice and its adhesion to metal and polymer surfaces has been investigated for several decades.[9]

Approaches for anti-icing (*viz.* preventing frost formation on surfaces) and de-icing (*viz.* removal of deposited ice) include passive solutions such as coatings and active techniques such as the application of heat, chemicals or mechanical shear.[10] For example, propylene glycol is sprayed on aircraft surfaces in a time-consuming, expensive and environmentally problematic[11] process to effect anti-icing/de-icing.[12,13] Other strategies such as mechanical agitation or scraping for removal of ice[14] have also been reported in the literature. Exciting new work shows that hybrid solutions that combine active and passive techniques can yield efficient, durable, low-power de-icing solutions.[15,16] For example, it has been shown that integrating passive coatings[17–19] with active methods is a promising approach to icephobic surfaces. However, even in such hybrid systems, the "base" passive coating critically determines overall performance. Currently available passive coatings still face challenges in maintaining durable performance over repeated icing–deicing cycles. Therefore, improved passive coatings that function simultaneously as anti-icing and de-icing agents, while also

Department of Chemical Engineering, IIT Bombay, Powai, Mumbai 400076, India. E-mail: dasgupta.ratul@iitb.ac.in, guruswamy@iitb.ac.in

being durable to repeated frosting cycles and to mechanical wear, remain important.

The mechanism of ice formation and deposition plays an important role in the design of ice-phobic (also called pagophobic) coatings. The formation of ice on solid surfaces can occur *via* two distinct routes: (a) solidification of supercooled water droplets on surfaces at temperatures below the freezing point and (b) direct ice condensation from the vapor phase of a highly humid environment.[20] Both routes need to be considered when designing an effective ice-phobic coating for the surface. Our study is organised as follows: we briefly review the literature on various approaches to preparing ice-phobic coatings. We then describe the preparation and testing of coatings based on these reported approaches. Finally, we describe the preparation of a novel pagophobic coating, that has excellent anti-icing and de-icing properties and that is robust to repeated frost/thaw cycles.

Super-hydrophobic surfaces (SHS)

Studies of the freezing of impacting droplets on SHS[21,22] provided support for the idea that superhydrophobicity could be employed to roll off impinging droplets before they could freeze on the surface, effective for surface temperatures as low as ≈−25 °C. We refer the reader to several perspective articles[23–25] that provide succinct overviews of the use of SHS coatings to prepare icephobic surfaces.

The use of SHS to prevent ice accretion does, however, face challenges. A static drop on an SHS coating can exist in either the Cassie state (droplet sitting atop rough asperities with minimal contact with the surface) or the Wenzel state (when the liquid drop penetrates the rough surface to make conformal contact). The ease of removal of liquid drops from SHS before they freeze is applicable only for drops in the Cassie state (but not in the Wenzel state, due to large contact angle hysteresis in this case). The study by Lafuma and Quéré[26] had already demonstrated a few years before Meuler *et al.*,[27] that a static droplet could transition irreversibly from the Cassie to the Wenzel state and when this occurred, dislodging droplets and the resultant ice from SHS would become difficult. It was also subsequently demonstrated[28] that under high relative humidity conditions associated with frost formation, the ice adhesion strength of SHS was higher than on smooth surfaces of the same material. Rough SHS surfaces exhibit higher surface area due to the incursion of ice into surface pockets, by displacing air. Thus, the area for ice-surface contact increases, consequently increasing the ice adhesion strength.

Liquid infused surfaces (SLIPS)

The formulation of slippery liquid infused porous surfaces[29] (referred to as SLIPS) represents an important advance in ice-phobic coatings. A perspective article by Stone[30] highlighted the development of pagophobic liquid infused surfaces,[29] as an alternative to SHS. Here, a hydrophobic liquid lubricant is infused on a hydrophobized rough substrate to generate a smooth, slippery water-repellent fluid surface. Such surfaces are characterized by very small contact angle hysteresis and very low ice adhesion strength. While SLIPS provide effective anti-icing initially, there is a deterioration in performance over successive freeze–thaw cycles. It is believed that this results from the removal of the low surface energy liquids infused into the surface, rendering the SLIPS coating ineffective.[31–33]

Stress localised surfaces/fracture controlled surfaces (SLS/FCS)

Recently, another category of icephobic surfaces has been developed based on elastomeric coatings.[34] This was inspired by the experimental study of Chaudhury *et al.*[35] as well as related earlier studies,[36] which probed the adhesion stress on such elastomeric surfaces. Chaudhury *et al.* observed that during the separation of a glass block from an elastomer film (PDMS), a fingering instability always develops at the contact line. Thus, the film is more compliant near the contact line region than in other regions of the confined film. In this case, the increase in the amplitude of the fingers controls the loss of interfacial contact, which further leads to catastrophic crack growth at a later stage. When a force is applied just above the interface, the critical stress required to de-bond a material from the surface of an elastomer is given by.

$$\sigma_s \sim \frac{a}{l}\sqrt{\frac{W_a G}{h}} \quad (1)$$

where W_a is the work of adhesion, G is the shear modulus of the film, h its thickness, a is the width of the material, and l is the distance from the bottom where the force is applied to debond the material. Chaudhury *et al.*[35] clearly distinguish this from the case of coatings where there is no elastic instability. In this case, the critical stress for debonding due to crack propagation is given by:

$$\sigma_s \sim \frac{a^2}{hl}\sqrt{\frac{W_a G}{h}} \quad (2)$$

The above relations suggest that by reducing G one may reduce the critical stress necessary for debonding ice. Golovin *et al.*[34] demonstrated that by tuning the cross-link density of elastomers, durable coatings with $\sigma_s < 10$ kPa could be maintained over one hundred icing de-icing cycles. Dhyani *et al.*[37] have recently reviewed the different kinds of coatings that have been developed. A drawback of using a low shear modulus material is that reduction in G also decreases the mechanical durability of the surface rendering it prone to mechanical abrasion. To address this shortcoming, Irajizad[38] has proposed coatings with a two-phase structure. They demonstrate that the connection between ice adhesion strength and the shear modulus of the film can be decoupled for coatings with a low shear modulus organogel phase that comes into contact with ice and a high shear modulus elastomer phase that provides the surface with mechanical durability. As these surfaces induce adhesive fracture by

creating artificial stress localization at specific points on the surface, the authors term these as stress localized surfaces (SLS).

Freezing point depressants

We had previously mentioned that aircraft exteriors are sprayed with propylene glycol to inhibit ice formation. Glycols are water miscible and depress the ice freezing point. Researchers have investigated anti-icing coatings based on freezing point depressants. Chatterjee *et al.*[39] compared the performance of various freezing point depressants as anti-frosting coatings. Among these materials, DMSO, which is highly hydrophilic and soluble in water, outperforms other chemicals. Diffusion of DMSO into the condensed water droplets lowers the freezing point of the water and hence leads to a delay in frosting. However, due to its highly hygroscopic nature, direct application of DMSO on micro/nanostructured rough surfaces can result in significant moisture absorption from the atmosphere, leading to dilution of the infused DMSO and a subsequent reduction in defrosting efficiency.

Recently, ice-phobic DMSO-based creams and gels have been prepared using surfactants and gelling agents.[40] These gels and creams are more durable than the direct infusion of DMSO into an SHS. DMSO-based gels can delay frost formation for an extended time compared to SHS and SLIPS. The encapsulation of DMSO into a polymeric organogel helps prevent rapid loss of DMSO. Its low vapor pressure, when compared to water, and its ability to form hydrogen bonds with water in a gel network render these gels stable. These gels can prevent frost formation for an extended period. Hence, they perform very well as anti-icing coatings. However, we show in the next section that they perform poorly for repeated freeze thaw cycles.

Anti-icing and de-icing performance of existing coatings

One of the challenges with comparing the performance of different icephobic coatings is the lack of standardized test protocols for the data reported in the literature. Table 1 summarizes the various test conditions used in the literature and the performance metrics obtained for a variety of coatings. This has prompted recent efforts to develop uniform metrics.[20] Moreover, as previously mentioned, the efficacy of anti- and de-icing coatings is a function of the conditions under which frost forms.[4]

Therefore, to assess the performance of SHS, SLIPS, SLS coatings and to contrast our work with the literature, we prepare coatings using reported protocols and test all coatings under similar conditions. SHS,[41] SLIPS,[42] SLS,[38] and gels of freezing point depressants[40] are prepared according to protocols described in the literature. The preparation of these coatings is described in detail in the SI (section I). The protocols used to test anti-icing and de-icing are described in the following section. Briefly, anti-icing is measured by observing the onset of frost formation when the coated substrate at ambient conditions of 28 °C and 60% relative humidity is cooled to −20 °C using a Peltier. De-icing efficacy is assessed by measuring the stress required to debond a standard frozen sample from the coated substrate (as described in the methods section).

Fig. 1(a) shows the time-dependent increase in frost coverage of substrates cooled to −20 °C and exposed to ambient conditions (28 °C, 60% RH). Data is presented for the case when freshly prepared substrates are subjected to frosting conditions for the first time. The uncoated aluminum surface is completely frosted within about 5 minutes. The time taken for frost formation on aluminum with SLS is only marginally higher, indicating the poor anti-icing performance of SLS. In comparison, aluminum with SHS coating is completely frosted in about 12 minutes, while

Table 1 Summary of literature reports of the performance of icephobic coatings and the test conditions employed

Icephobic coatings	Test conditions	Anti-icing/de-icing performance	Ref.
SHS	Frosting at: Surface temperature = −10 °C, Room conditions = 22 °C, 25–30% RH	Completely frosted within 11 min	31, 32
	IAS – Centrifugal force	IAS(−5 °C) = 12 ± 3 kPa IAS(−15 °C) = 30 ± 5 kPa IAS(−30 °C) = 253 ± 18 kPa	
SLIPS	Frosting at: Surface temperature = −10 °C, Room conditions = 22 °C, 25–30% RH	Completely frosted within 24 minutes	31, 43
	IAS – Translation force, Shear rate = 0.5 mm s^{-1}	IAS(−10 °C) = 22 ± 5 kPa IAS(−20 °C) = 35 ± 15 kPa No cyclic de-icing tests were performed	
SLS	Data for frosting tests are not available	IAS: 10–50 kPa	38, 44
	IAS – Translation force, Shear rate = 0.1 mm s^{-1}, Surface temperature = −25 °C, Coating thickness = 300 μm	Cyclic de-icing tests showed a negligible increase in IAS	
Freezing point depressant infused gel coatings	Frosting at: Surface temperature = −30 °C, Room conditions = 24 °C and 60–90% RH, Coating thickness = 1.5 mm	Time for 100% frosting (1st cycle) = 300 min Time for 100% frosting decreased to 45 min in subsequent cycles	40
	IAS – Translation force, Shear rate = 0.1 mm s^{-1}, Surface temperature = −15 °C, RH = 10%, Coating thickness = 1.5 mm	Average IAS = 20 kPa Cyclic de-icing tests showed a 33% increase in IAS by 10th cycle	

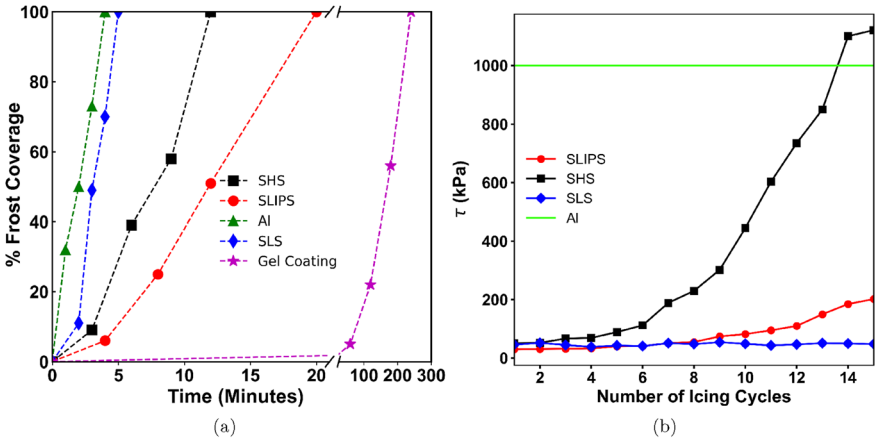

Fig. 1 (a) Time dependent frost coverage of the substrate: data for bare aluminum (Al), and Al coated with superhydrophobic (SHS), slippery liquid infused porous (SLIPS), stress localized (SLS) or ethylene glycol gel. Frosting conditions employed are: substrate temperature = −20 °C, room conditions = 28 °C and 60% RH, coating thickness of SLS and ethylene glycol gel coatings ~1 mm. The error bars are smaller than the marker size (b) variation of ice adhesion stress (IAS) of SHS, SLIPS, and SLS with the number of icing cycles (surface temperature = −20 °C). The protocol of IAS measurement is described in the methods section.

SLIPS is more effective, delaying complete frost coverage to ≈20 minutes. Compared with these, the ethylene glycol gel exhibited significantly superior performance, with complete frosting at about 240 minutes. We have also prepared gels using DMSO as the freezing point depressant. These gels behave in a qualitatively similar manner to ethylene glycol gel. This data is presented in the supporting information (Fig. S4).

Fig. 1(b) demonstrates the change in ice-adhesion stress (IAS) for the different substrates and coatings over multiple freeze–thaw cycles. The bare aluminum surface shows a very high ice adhesion stress (≈1 MPa), that does not change much with repeated freeze–thaw cycles. Initially, the coated substrates all exhibited a relatively low ice adhesion stress (about ≈50 kPa for SHS, ≈30 kPa for SLIPS, and ≈45 kPa for SLS). However, with repeated freeze–thaw cycles, the IAS for SHS and SLIPS showed a systematic increase (Fig. 1b). This is consistent with the literature: for SHS, an increase in IAS has been attributed to a change in the wetting state from Cassie to Wenzel as mentioned previously. This increases the surface contact area between the surface and the condensed water droplet. Upon frosting, these condensed water droplets damage the multi-scale textures on the SHS and cause an increase in IAS.[28] Note that after a certain number of cycles, the IAS of SHS is even above that of the aluminum surface (Fig. 1b). This may be due to the higher contact area between the roughened (higher effective surface area) SHS and ice in comparison with the smooth aluminum surface. In the case of SLIPS, the gradual depletion of the lubricant from the surface can lead to direct exposure of the aluminum surface to the highly humid atmosphere, thereby increasing the IAS of SLIPS with the number of icing cycles.[31] The SLS shows superior de-icing properties compared to the other surfaces, *i.e.*, the IAS values on SLS don't change much over fifteen repeated cycles (Fig. 1b). This superior performance is attributed to the stress localization effect as described previously. We note that while the SLS coating provides excellent de-icing properties, its performance is very poor when it comes to delaying frost formation (Fig. 1a).

We now evaluate the robustness of the anti-icing performance of the ethylene glycol gel coating by performing repeated frosting cycle tests, each lasting one hour. The experimental conditions were the same as those used in the initial frosting tests, *viz.* the coated substrate was cooled to −20 °C and exposed to ambient conditions of 28 °C and 60% RH. The percentage of frost coverage formed in an hour on the ethylene glycol gel coated substrate for repeated cycles is shown in Fig. 2. We observed that the gel coating delayed complete frost coverage to 240 minutes (Fig. 1a). In the first cycle, less than 30% of the surface is frosted in an hour. However, its effectiveness diminishes significantly in subsequent cycles. In the second cycle, 70% of the coated surface was frosted in an hour, and the entire surface was frosted within an hour in the third cycle (Fig. 2).

Thus, there is a need for novel ice-phobic coatings that combine anti-icing with de-icing, and that are robust to repeated freeze–thaw cycles. This is the focus of the present work. Here, we present a coating that combines the remarkable anti-icing performance of freezing point depressants with the de-icing capabilities of SLS, and is able to maintain ice-phobicity over several freezing cycles.

Materials and methods

Ethylene glycol, sodium bis(2-ethylhexyl) sulfosuccinate (AOT) surfactant, hexane (99% pure, analytical grade) glutaraldehyde (grade II, 25% in water), gelatin (from bovine skin, type B, gel strength ~225 g bloom), dimethyl sulfoxide (DMSO) (analytical grade), 1*H*,1*H*,2*H*,2*H*-perflouro-octotriethoxysilane (99% pure, analytical grade), hexadecyltrimethoxysilane (HDTMS) (technical, >85%), silicone oil (viscosity 25 cSt at 25 °C), were obtained from

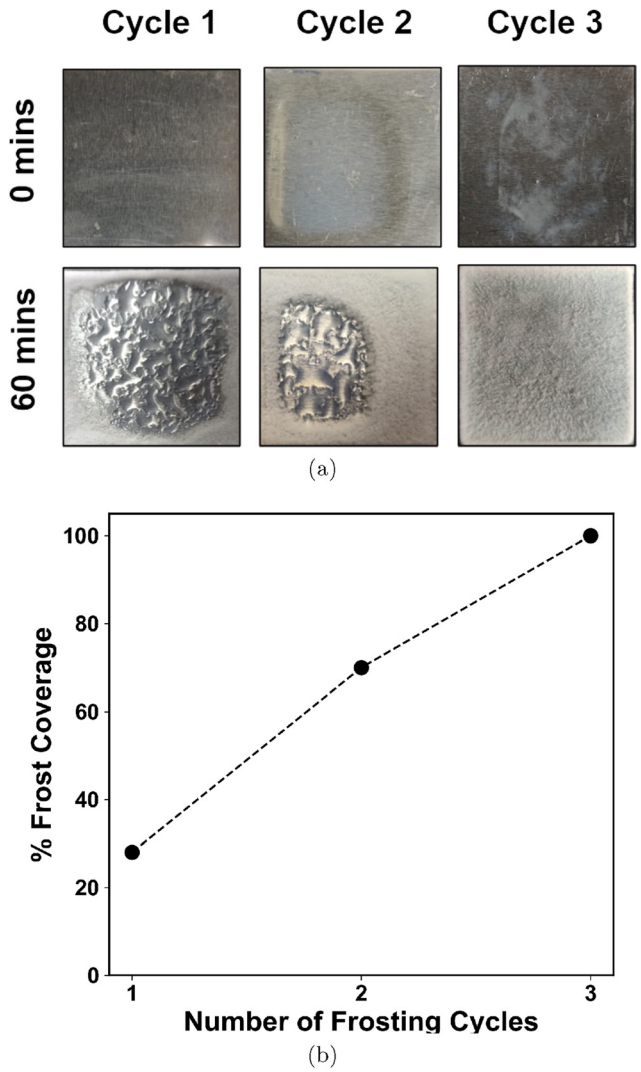

Fig. 2 (a) Time taken for 100% frost coverage on the ethylene glycol coating with the repeated frosting experiments (b) frost coverage on ethylene glycol gel coating with the number of frosting cycles of 1 h each. Frosting conditions employed are: Surface temperature = −20 °C, room conditions = 28 °C and 60% RH, coating thickness = ~1 mm.

Sigma Aldrich and used without purification, store bought RTV-1 silicone was used. Aluminum sheets (8000 series) were purchased from a local store and cut into 4 cm × 4 cm pieces and used as substrates for the frosting experiments.

We first describe the preparation of a novel coating, which is referred to as E-ICE (Fig. 3, E refers to emulsion) hereafter. In this coating, a hydrophobic matrix phase (phase I) encapsulates a dispersed phase (phase II) that is hydrophilic. Hence, the phases do not readily mix. To promote compatibility, a surfactant (AOT) is added to phase I (silicone matrix) along with a chemical cross-linker whose role is to cross-link phase II dispersed in the matrix. Phase II, therefore, comprises crosslinked soft hydrogel particles swollen with freezing point depressant. The presence of the surfactant leads to the formation of a mini-emulsion of phase II gel particles in a phase I matrix. This emulsion is coated on the aluminum surface and allowed to cure at room temperature. The chemical cross-linker leads to the cross-linking of phase II, while the silicone matrix phase is crosslinked thermally at room temperature. Thus, both phases I and II are cross-linked *in situ* in this coating (Fig. 3).

Preparation methodology

An example of the preparation of E-ICE coating is as follows. Gelatin (0.833 g) is dissolved in 10 mL ethylene glycol–water mixture (50 : 50 v/v) with gentle heating and vigorous stirring. This forms the dispersed phase (phase II) of the coating. Separately, 2 g of RTV-1 silicone is dissolved in 10 mL of *n*-hexane, and 0.4 g of AOT surfactant is added to the silicone solution. The mixture is stirred continuously in a 100 mL beaker with a PTFE-coated stir bar rotated using a magnetic stirrer set at 400 rpm until a homogeneous solution is obtained. Then, 10 μL of glutaraldehyde solution is added to this mixture. The as prepared phase II solution is then added dropwise to phase I with vigorous stirring. Dropwise addition and continuous stirring are necessary to ensure that a stable mini-emulsion is formed, without phase separation between hydrophobic and hydrophilic phases. Here, phase II comprises AOT stabilized gelatin hydrogel particles crosslinked by glutaraldehyde and swollen with ethylene glycol. The continuous matrix phase (phase I) is crosslinked silicone.

Rheology of the coating and the image analysis of the optical micrographs are described in sections VIII and III, respectively, of the SI.

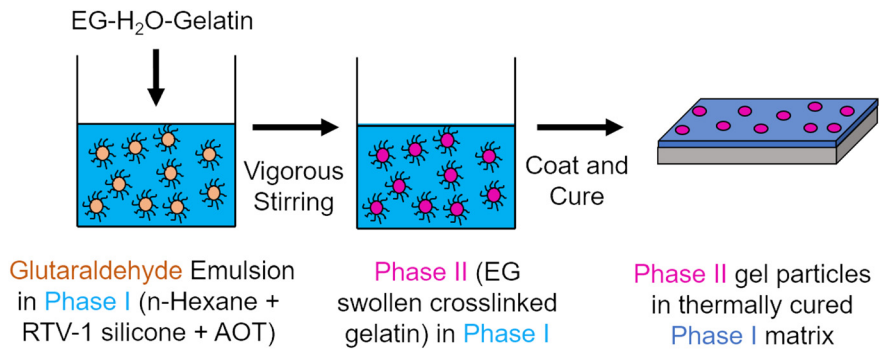

Fig. 3 Schematic of preparation of E-ICE coating.

Frosting experiment

This experiment used a thermoelectric Peltier module (TEC1-12706, LabsGuru Technologies Pvt Ltd, India) with dimensions 4 cm × 4 cm to cool the substrate. The module operates by converting electrical power into a thermal gradient across its surfaces, and the hot side requires continuous heat dissipation to maintain the temperature differential for cooling. To achieve a substrate temperature of −20 °C, an aluminum water cooling block was utilized to extract heat from the module's hot side *via* circulating cold water. This ensured stable performance and prevented overheating. The Peltier module was operated at its maximum rated capacity of 12 V and 5A, powered by a variable DC power supply (SPS305, Dhruv Pro Nice Power, India; output voltage 0–30 V at a resolution of 0.01 V, output current: 0–5 A at a resolution of 0.001 A). Both the cooling water temperature and the power input to the module were optimized to maintain a stable temperature of the substrate at −20 °C. Ambient conditions during the experiments were 28 °C with 60% relative humidity (RH). A K-type thermocouple was used to measure the temperature of the substrate with an accuracy of ±1 °C. The frost formation process on the 4 cm × 4 cm substrate was continuously monitored using a Dino-Lite digital microscope (model no. AF4915ZTL, resolution: 1280 × 1024, magnification 5×) to observe the time taken for complete surface frosting. The procedure for quantifying the % frost coverage is described in the supplementary information (Fig. S1).

Ice adhesion measurement protocol

The ice adhesion stress (IAS) is measured on each of the substrates by measuring the force required to detach a water-filled plastic cuvette frozen on the surface. As shown in Fig. 4, a 1 kg load cell is attached to the horizontal moving arm of the 3D printer. The output from the load cell was rated at 2.0 ± 0.15 mV V^{-1}. Since the output from the load cell was in millivolts, an instrumentation amplifier with an analog-to-digital converter (HX711) was used to read the output using an Arduino™ microcontroller. The load sensor is calibrated using known weights before performing the stress measurement experiments. A plastic cuvette is filled with water and placed upside down onto the 4 cm × 4 cm substrate. The substrate is cooled down to −20 °C using the Peltier module as described previously. After the water inside the cuvette is frozen completely, the substrate is moved toward the load cell at a speed of 1 mm s^{-1}. The force required to detach the cuvette of ice completely was measured using the load cell. The force obtained was divided by the cross-sectional area of the cuvette to get the IAS.

Results & discussion

Anti-icing performance of E-ICE coating

E-ICE coated aluminum substrates perform significantly better than its counterparts (Fig. 1a), preventing complete frost formation for more than 200 minutes. As shown in Fig. 5a, dropwise condensation occurs on the surface with time, and these droplets merge to form bigger droplets. These condensed water droplets freeze to form ice after a long period (over 200 minutes, Fig. 5b). Coatings containing freezing point depressant, ethylene glycol, E-ICE, as well as the gel coating, delay frost formation significantly longer than any of the other coatings. These results suggest that the gradual diffusion of ethylene glycol into the condensed water droplets lowers the freezing point of water and delays frost formation.

Next, we evaluate the robustness of the E-ICE coating to repeated frosting cycle tests. We subject aluminum substrates coated with E-ICE to repeated frosting cycles, each lasting one hour. The experimental conditions were the same as those used in the other frosting trials. The fraction of E-ICE coated substrate covered by frost after exposure to −20 °C for an hour is shown in Fig. 6a. The fraction of substrate frosted for each subsequent freezing cycle is shown in Fig. 6b. E-ICE coated substrates demonstrate durability to repeated frost-thaw cycles even under the harsh conditions of the test, with ≈25% of the area getting frosted after five consecutive freezing cycles. In contrast, the anti-icing effectiveness of

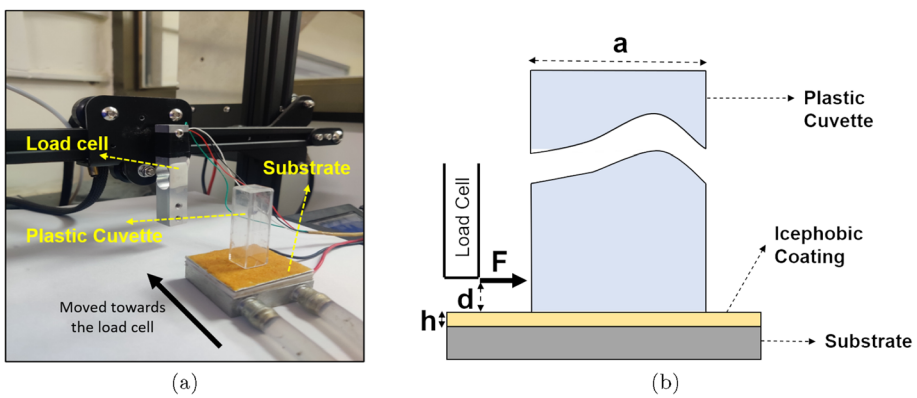

Fig. 4 (a) Setup for measuring ice adhesion stress (IAS) values (b) schematic for measurement of ice adhesion stress (IAS), where d is the distance from the interface where the force F is applied, h is the thickness of the coating, and a is the width the plastic cuvette. The values of d, a, and h are selected such that $a/h > 1$ and $d/a < 1$. For this experiment, a = 10 mm, d = 2 mm, $h \approx 1$ mm, and the shear rate at which the force F is applied at a shear rate of 1 mm s^{-1}. (Rough schematic not to scale).

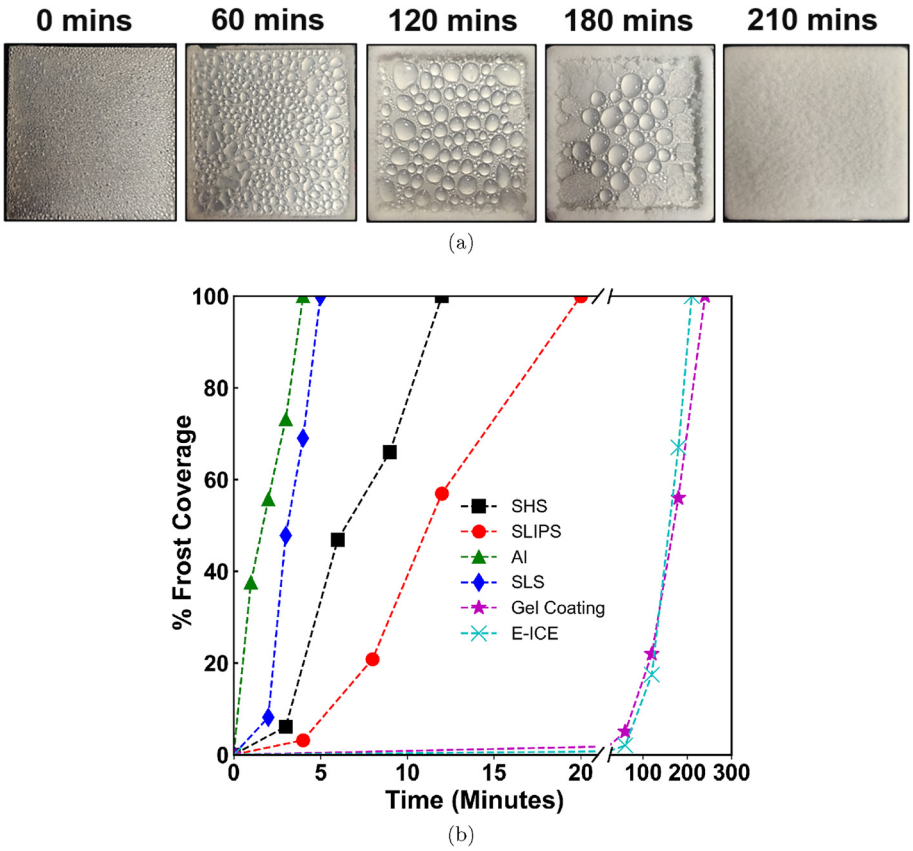

Fig. 5 (a) Time-dependent frost coverage on E-ICE coating with time. (b) Comparison of time-dependant frost coverage of E-ICE with aluminum (Al), and Al coated with superhydrophobic (SHS), slippery liquid infused porous (SLIPS), stress localized (SLS) and ethylene glycol gel. Frosting condition employed are: substrate temperature = −20 °C room conditions = 28 °C and 60% RH, coating thickness of SLS, ethylene glycol gel and E-ICE = ~1 mm. The error bars are smaller than the marker size.

gel-coated substrates diminished significantly after the first cycle. Ethylene glycol gel coated surfaces showed 70% frosting after the second cycle and complete frosting at the end of the third cycle (Fig. 2b). We attribute the improvement in anti-icing robustness over repeated cycles for E-ICE to the structure of the coating, where the ethylene glycol swells the dispersed hydrogel particles (phase II) encapsulated in a hydrophobic silicone matrix (phase I). We have also prepared coatings where AOT-stabilized ethylene glycol droplets are directly dispersed (rather than in gelatin hydrogel particles) in a silicone matrix (see SI section V). These coatings do not exhibit the same level of robustness to repeated freeze–thaw cycles as E-ICE. Therefore, incorporating the ethylene glycol within a crosslinked gelatin particle phase, and dispersing these swollen hydrogel particles in a hydrophobic silicone matrix, are both important structural features of the coating that confer robustness to repeated freeze–thaw cycles.

The approach of using an encapsulated freezing point depressant is general, and is not limited to the use of ethylene glycol. We note that concerns about potential health hazards from exposure to ethylene glycol used for deicing aircraft have prompted studies,[45] that concluded that the typical concentrations encountered in these applications were insufficient to cause acute or chronic kidney damage in workers. However, they stated that prolonged exposure in the absence of appropriate safety protocols can pose health risks. Further comparative risk assessments between ethylene glycol and other anti-icing fluids, such as propylene glycol, have shown propylene glycol to be more environmentally benign.[46] While the search for safer and more sustainable anti-icing fluids continues, we have importantly demonstrated the versatility of our coating formulation by substituting ethylene glycol with dimethyl sulfoxide (DMSO) as the freezing point depressant. This coating exhibited excellent anti-frosting properties, comparable to E-ICE coatings. However, preliminary experiments suggest that E-ICE coatings are more robust in preventing frost formation. We attribute this difference to the high hygroscopic nature of DMSO, which promotes faster diffusion into condensed water droplets compared to ethylene glycol (SI, Fig. S4). We note in passing that we have also prepared two-phase coatings by pre-crosslinking DMSO encapsulated gelatin gels and subsequently adding them to a silicone matrix. This coating was cured by exposure to UV radiation. Exposure to UV did not result in deterioration of the performance of the coating. While this coating showed excellent de-icing and anti-icing performance, inclusion of pre-formed gel particles resulted in a higher surface roughness. Therefore, we do not focus on this in the current study. Details of the

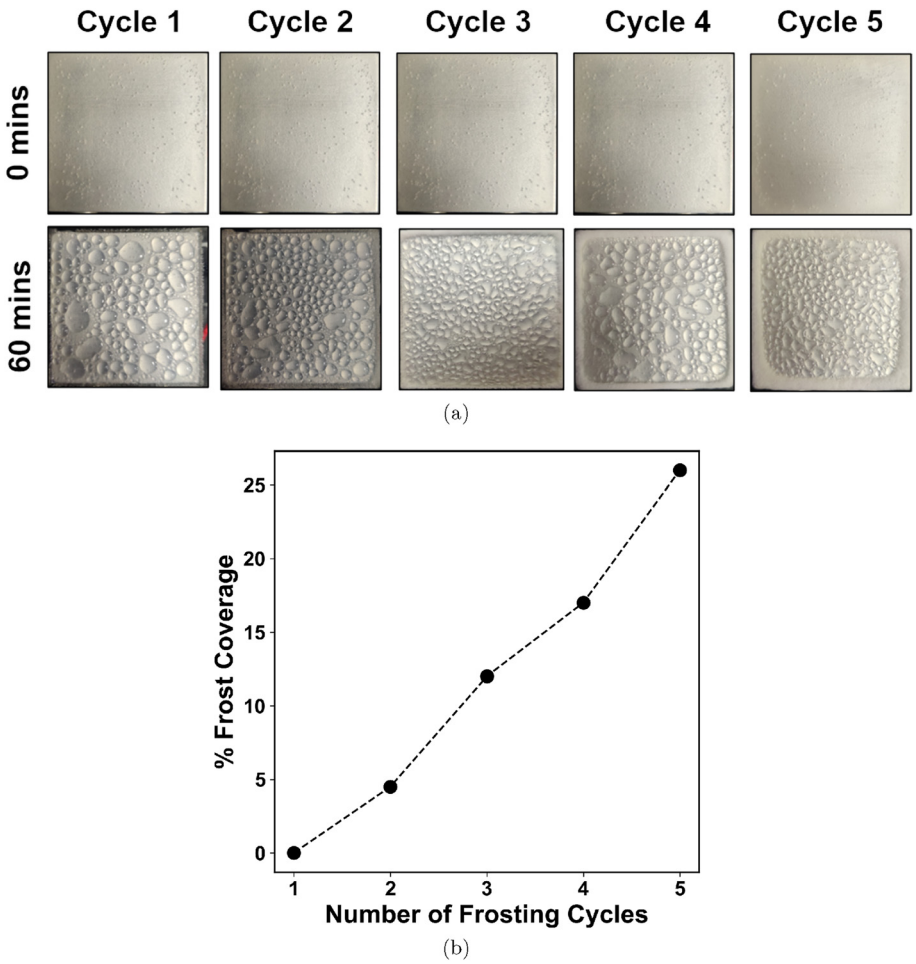

Fig. 6 (a) Anti-icing performance of E-ICE coating under multiple freeze–thaw cycles. Frosting conditions employed are: surface temperature = −20 °C, room conditions = 28 °C and 60% RH, cycle time = 60 min. The first row depicts the surface at the start of the cycle while the second row depicts the surface at the end of the 60 min cycle (b) quantitative representation of % frost coverage on E-ICE with the number of cycles.

preparation and pagophobic response of this material are given in the SI (Fig. S6).

De-icing properties of E-ICE

Having described the anti-icing property of E-ICE, we now describe its de-icing behavior. The ice adhesion stress (IAS) values of E-ICE coating over a number of freeze–thaw cycles are shown in Fig. 7. We observed that the IAS of E-ICE is very low (≈6 kPa) in comparison to the substrates described previously. (Fig. 1b). Importantly, E-ICE coated substrates can maintain low IAS values for over 15 cycles as shown in Fig. 7. Like SLS, the E-ICE coating also comprises soft gel dispersed in a rigid matrix phase. In both cases, the coating exhibits low IAS. However, the absolute IAS of the E-ICE coating is lower than that of the SLS coating. Suppose stress localization, as described by Chaudhary *et al.*, is the mechanism driving the shearing process of ice on the substrate, the IAS value should depend solely on the shear modulus of phase II for coatings of the same thickness. Contrary to this expectation, we find that although the shear modulus of phase II for SLS (≈400 kPa) is lower than that of E-ICE (≈600 kPa) (see SI, Fig. S8b), E-ICE still exhibits a significantly lower IAS value.

Hence, to investigate the deicing mechanism, we examine the thickness dependence of the interfacial adhesion strength (IAS) in Fig. 8. Experiments were conducted with a five-fold variation in coating thickness, ranging from 300 μm to 1500 μm. We observe that the scaling exponent of IAS with h is closer to −1.5 than −0.5. As discussed in the introduction (eqn (1)), this suggests that debonding is not driven by elastic instability. Notably, in experiments with E-ICE, the frozen cuvette slides on the coating during debonding. In contrast, the cuvette tilts when debonded from SHS and SLS coatings but slides on SLIPS. This behavior indicates the presence of a liquid lubricating layer on the surface of E-ICE, likely formed due to the inhibition of ice formation at the interface by freezing point depressants. Remarkably, the encapsulation of these freezing point depressants results in robust coatings where low IAS values are maintained over many cycles, as shown in Fig. 7. This contrasts with SLIPS, where lubricant depletion leads to increased IAS values over repeated cycles, as evident in Fig. 1(b).

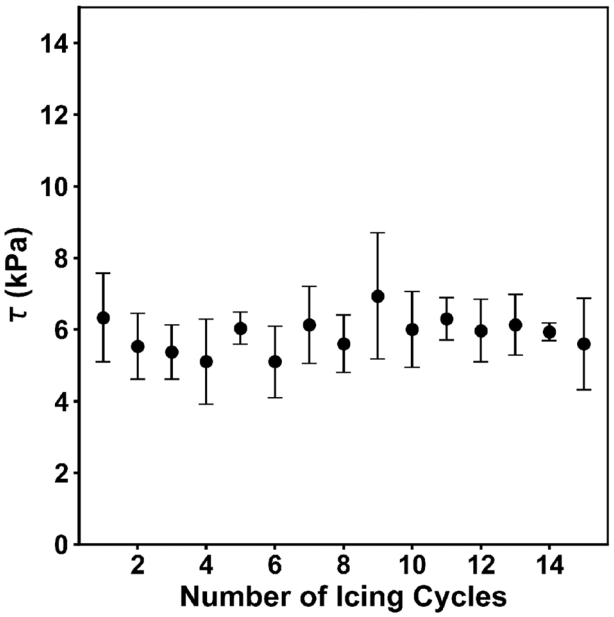

Fig. 7 Variation of ICE adhesion stress (IAS) of E-ICE coating with the number of icing cycles. Experiments were performed at, surface temperature = −20 °C, and coating thickness = ~1 mm.

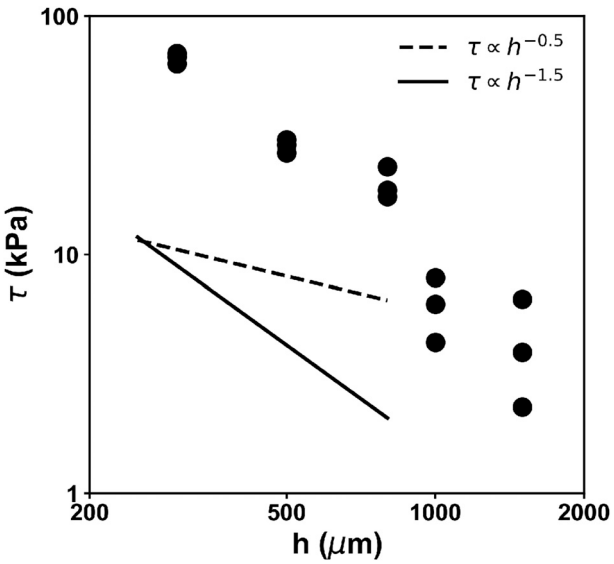

Fig. 8 Variation of ICE adhesion stress (IAS) of E-ICE coating with the thickness of the coating. Experiments were performed at the surface temperature of −20 °C, and the coating thickness was varied as indicated.

Conclusions

We describe a two phase coating, E-ICE, that combines a soft gelatin gel swollen with freezing point depressant, ethylene glycol, encapsulated in a hydrophobic silicone matrix. Application of this coating renders aluminum surface anti-icing, with frost formation delayed to several hours, and de-icing, characterized by low adhesion stress of a few tens of kPa. These exceptional properties are retained over multiple freeze thaw cycles, indicating the robust performance of this coating. We have contrasted the performance of this coating to those reported in the literature (superhydrophobic, SLIPS, stress-localizing surfaces, antifreeze gels), and show that, under the same frosting conditions, E-ICE shows significantly improved anti-icing and de-icing performance over multiple freezing cycles. This coating represents a promising solution in demanding environments for applications requiring reliable and efficient frost suppression and de-icing performance.

Conflicts of interest

The manuscript forms the basis for a granted patent (Patent No: IN517107).

Data availability

Methods of preparation of other coatings from the literature, characterization of E-ICE coating, ImageJ analysis for quantifying frost coverage and pagophobic performance of E-ICE coating with DMSO as freezing point depressant are available in SI. See DOI: **https://doi.org/10.1039/D5LF00181A**.

The plots and figures in this manuscript reflect the original data. Raw files associated with the data presented in this work will be made available on reasonable request.

Acknowledgements

This work was supported, in part, by Honeywell Technology Solutions (HTS), Pvt. Ltd., India. We gratefully acknowledge collaboration and discussions with the team from HTS.

References

1 H. Sojoudi, M. Wang, N. Boscher, G. H. McKinley and K. K. Gleason, Durable and scalable icephobic surfaces: similarities and distinctions from superhydrophobic surfaces, *Soft Matter*, 2016, **12**, 1938–1963.
2 X. Huang, N. Tepylo, V. Pommier-Budinger, M. Budinger, E. Bonaccurso, P. Villedieu and L. Bennani, A survey of icephobic coatings and their potential use in a hybrid coating/active ice protection system for aerospace applications, *Prog. Aerosp. Sci.*, 2019, **105**, 74–97.
3 A. Dhyani, J. Wang, A. K. Halvey, B. Macdonald, G. Mehta and A. Tuteja, Design and applications of surfaces that control the accretion of matter, *Science*, 2021, **373**, eaba5010.
4 M. J. Kreder, J. Alvarenga, P. Kim and J. Aizenberg, Design of anti-icing surfaces: smooth, textured or slippery?, *Nat. Rev. Mater.*, 2016, **1**, 1–15.
5 A. R. Solangi, Icing effects on power lines and anti-icing and De-icing methods, *M. Sc. thesis*, UiT The Arctic University of Norway, 2018.
6 BEA, Final Report: Accident to Airbus A330–203 registered F-GZCP, Air France AF 447 Rio de Janeiro – Paris, 1st June 2009. 2014; **https://aaiu.ie/sites/default/files/FRA/BEA%20France%**

20Accident%20Airbus%20A330-203%20F-GZCP%20AF447%20Atlantic%20Ocean%2001-06-2012_opt.pdf.
7 L. D. Stone, C. M. Keller, T. M. Kratzke and J. P. Strumpfer, Search for the wreckage of Air France Flight AF 447, *Stat. Sci.*, 2014, **29**, 69–80.
8 How Statisticians Found Air France Flight 447 Two Years After It Crashed Into Atlantic, *MIT Technology Review*, 2014, https://www.technologyreview.com/2014/05/27/13283/how-statisticians-found-air-france-flight-447-two-years-after-it-crashed-into-atlantic/.
9 L. Raraty and D. Tabor, The adhesion and strength properties of ice, *Proc. R. Soc. London, Ser. A*, 1958, **245**, 184–201.
10 M. Farzaneh, C. Volat and A. Leblond, *Atmospheric icing of power networks*, Springer, 2008, pp. 229–268.
11 R. West, M. Banton, J. Hu and J. Klapacz, The distribution, fate, and effects of propylene glycol substances in the environment, *Rev. Environ. Contam. Toxicol.*, 2014, **232**, 107–138.
12 Air Force Aircraft and Airfield Deicing/Anti-icing, 1998, https://p2infohouse.org/ref/01/00593.pdf.
13 E. K. Sam, D. K. Sam, X. Lv, B. Liu, X. Xiao, S. Gong, W. Yu, J. Chen and J. Liu, Recent development in the fabrication of self-healing superhydrophobic surfaces, *Chem. Eng. J.*, 2019, **373**, 531–546.
14 L. Zhou, R. Liu and X. Yi, Research and development of anti-icing/deicing techniques for vessels, *Ocean Eng.*, 2022, **260**, 112008.
15 H. Gao, Y. Zhou, J. Ma, H. Jin, J. Bao and D. Wen, Recent advancements in electro-thermal anti−/de-icing materials, *RSC Adv.*, 2025, **15**, 17102–17115.
16 R. Rekuviene, S. Saeidiharzand, L. Mažeika, V. Samaitis, A. Jankauskas, A. K. Sadaghiani, G. Gharib, Z. Muganlı and A. Koşar, A review on passive and active anti-icing and de-icing technologies, *Appl. Therm. Eng.*, 2024, **250**, 123474.
17 H. Wei, H. Luo, W. Fan, Y. Chen, J. Xiang and H. Fan, A passive-active anti/deicing coating integrating superhydrophobicity, thermal insulation, and photo/electrothermal conversion effects, *ACS Appl. Mater. Interfaces*, 2024, **16**, 35613–35625.
18 Z. Zhao, Y. Wang, Z. Wang, X. Cui, G. Liu, Y. Zhang, Y. Zhu, J. Chen, S. Sun and K. Zhang, *et al.*, A new composite material with energy storage, electro/photo-thermal and robust super-hydrophobic properties for high-efficiency anti-icing/de-icing, *Small*, 2024, **20**, 2311435.
19 Y. Wang, K. Zhang, X. Cui, Z. Zhao, Z. Wang, G. Liu, Y. Zhang, Y. Zhu, J. Chen and S. Sun, *et al.*, A transparent photo/electrothermal composite coating with liquid-like slippery property for all-day anti−/de-icing, *ACS Appl. Mater. Interfaces*, 2024, **16**, 41400–41408.
20 P. Irajizad, S. Nazifi and H. Ghasemi, Icephobic surfaces: Definition and figures of merit, *Adv. Colloid Interface Sci.*, 2019, **269**, 203–218.
21 L. Mishchenko, B. Hatton, V. Bahadur, J. A. Taylor, T. Krupenkin and J. Aizenberg, Design of ice-free nanostructured surfaces based on repulsion of impacting water droplets, *ACS Nano*, 2010, **4**, 7699–7707.
22 A. Alizadeh, V. Bahadur, S. Zhong, W. Shang, R. Li, J. Ruud, M. Yamada, L. Ge, A. Dhinojwala and M. Sohal, Temperature dependent droplet impact dynamics on flat and textured surfaces, *Appl. Phys. Lett.*, 2012, **100**, 111601.
23 W. Huang, J. Huang, Z. Guo and W. Liu, Icephobic/anti-icing properties of superhydrophobic surfaces, *Adv. Colloid Interface Sci.*, 2022, **304**, 102658.
24 J. Jeevahan, M. Chandrasekaran, G. Britto Joseph, R. Durairaj and G. Mageshwaran, Superhydrophobic surfaces: a review on fundamentals, applications, and challenges, *J. Coat. Technol. Res.*, 2018, **15**, 231–250.
25 X. Wu, V. V. Silberschmidt, Z.-T. Hu and Z. Chen, When superhydrophobic coatings are icephobic: Role of surface topology, *Surf. Coat. Technol.*, 2019, **358**, 207–214.
26 A. Lafuma and D. Quéré, Superhydrophobic states, *Nat. Mater.*, 2003, **2**, 457–460.
27 A. J. Meuler, G. H. McKinley and R. E. Cohen, Exploiting topographical texture to impart icephobicity, *ACS Nano*, 2010, **4**, 7048–7052.
28 K. K. Varanasi, T. Deng, J. D. Smith, M. Hsu and N. Bhate, Frost formation and ice adhesion on superhydrophobic surfaces, *Appl. Phys. Lett.*, 2010, **97**, 234102.
29 P. Kim, T.-S. Wong, J. Alvarenga, M. J. Kreder, W. E. Adorno-Martinez and J. Aizenberg, Liquid-infused nanostructured surfaces with extreme anti-ice and anti-frost performance, *ACS Nano*, 2012, **6**, 6569–6577.
30 H. A. Stone, Ice-phobic surfaces that are wet, *ACS Nano*, 2012, **6**, 6536–6540.
31 K. Rykaczewski, S. Anand, S. B. Subramanyam and K. K. Varanasi, Mechanism of frost formation on lubricant-impregnated surfaces, *Langmuir*, 2013, **29**, 5230–5238.
32 L. B. Boinovich, K. A. Emelyanenko and A. M. Emelyanenko, Superhydrophobic versus SLIPS: Temperature dependence and the stability of ice adhesion strength, *J. Colloid Interface Sci.*, 2022, **606**, 556–566.
33 H. Niemelä-Anttonen, H. Koivuluoto, M. Tuominen, H. Teisala, P. Juuti, J. Haapanen, J. Harra, C. Stenroos, J. Lahti and J. Kuusipalo, *et al.*, Icephobicity of slippery liquid infused porous surfaces under multiple freeze–thaw and ice accretion–detachment cycles, *Adv. Mater. Interfaces*, 2018, **5**, 1800828.
34 K. Golovin, S. P. Kobaku, D. H. Lee, E. T. DiLoreto, J. M. Mabry and A. Tuteja, Designing durable icephobic surfaces, *Sci. Adv.*, 2016, **2**, e1501496.
35 M. Chaudhury and K. Kim, Shear-induced adhesive failure of a rigid slab in contact with a thin confined film, *Eur. Phys. J. E:Soft Matter Biol. Phys.*, 2007, **23**, 175–183.
36 A. Ghatak, L. Mahadevan, J. Y. Chung, M. K. Chaudhury and V. Shenoy, Peeling from a biomimetically patterned thin elastic film, *Proc. R. Soc. London, Ser. A*, 2004, **460**, 2725–2735.
37 A. Dhyani, W. Choi, K. Golovin and A. Tuteja, Surface design strategies for mitigating ice and snow accretion, *Matter*, 2022, **5**, 1423–1454.
38 P. Irajizad, A. Al-Bayati, B. Eslami, T. Shafquat, M. Nazari, P. Jafari, V. Kashyap, A. Masoudi, D. Araya and H. Ghasemi, Stress-localized durable icephobic surfaces, *Mater. Horiz.*, 2019, **6**, 758–766.

39 R. Chatterjee, D. Beysens and S. Anand, Delaying ice and frost formation using phase-switching liquids, *Adv. Mater.*, 2019, **31**, 1807812.
40 R. Chatterjee, H. Bararnia and S. Anand, A Family of Frost-Resistant and Icephobic Coatings, *Adv. Mater.*, 2022, **34**, 2109930.
41 C. S. Sharma, J. Combe, M. Giger, T. Emmerich and D. Poulikakos, Growth rates and spontaneous navigation of condensate droplets through randomly structured textures, *ACS Nano*, 2017, **11**, 1673–1682.
42 T. Maitra, C. Antonini, M. A. der Mauer, C. Stamatopoulos, M. K. Tiwari and D. Poulikakos, Hierarchically nanotextured surfaces maintaining superhydrophobicity under severely adverse conditions, *Nanoscale*, 2014, **6**, 8710–8719.
43 S. Barthwal and S.-H. Lim, Rapid fabrication of a dual-scale micro-nanostructured superhydrophobic aluminum surface with delayed condensation and ice formation properties, *Soft Matter*, 2019, **15**, 7945–7955.
44 S. Nazifi, Z. Huang, A. Hakimian and H. Ghasemi, Fracture-controlled surfaces as extremely durable ice-shedding materials, *Mater. Horiz.*, 2022, **9**, 2524–2532.
45 P. Louchez, S. Bernardin and J.-L. Laforte, Physical properties of aircraft de-icing and anti-icing fluids, *36th AIAA aerospace sciences meeting and exhibit*, 1998, p. 575.
46 A. Yakovlieva, S. Boichenko, I. Shkilniuk, A. Bakhtyn, U. Kale and A. Nagy, Assessment of influence of anti-icing fluids based on ethylene and propylene glycol on environment and airport infrastructure, *Int. J. Sustain. Aviat.*, 2022, **8**, 54–74.